IEEE Access
Multidisciplinary | Rapid Review | Open Access Journal

Received February 20, 2021, accepted March 7, 2021, date of publication March 17, 2021, date of current version March 26, 2021.

Digital Object Identifier 10.1109/ACCESS.2021.3066464

An Improved S-Band CubeSat Communication Subsystem Design and Implementation

HAYTHEM HUSSEIN ABDULLAH, AYMAN ELBOUSHI, (Senior Member, IEEE), AHMED ESSAM GOHAR, AND ESMAT A. ABDALLAH, (Member, IEEE)
Electronics Research Institute, Giza 12622, Egypt

Corresponding author: Haythem Hussein Abdullah (haythm_eri@yahoo.com)

This work was supported in part by the Egyptian Space Agency (EgSA), and in part by the Electronics Research Institute (ERI), Egypt, in the project entitled S-Band CubeSat Communication Subsystem.

ABSTRACT In the past decade, the majority of the launched satellites have a weight exceeds 1 Ton. Its development takes a long time, high cost, and has a large risk of failure, and does not allow for testing new technologies to avoid the mission's failure. From these points of view, space-tested technologies were preferred to mitigate the risk of failure. Our goal is to build and test our own S-band communication subsystem for CubeSat. The system should be developed with reliable and compact hardware and flexible and efficient software. It consists of passive components such as the antennas and the filters and other active components. The passive components are designed, fabricated and measured while the active components are based on commercial components. In this paper, two antenna boards are designed; one board faces the earth and the other board lies on the opposite side. Each board has two antennas; transmitter and receiver antennas. The transmitter/receiver antennas are operating in the downlink /uplink at frequency bands from 2.2 GHz to 2.29 GHz and from 2.025 GHz to 2.11 GHz, respectively. This configuration keeps the communication between the CubeSat and the ground station to facilitate the de-tumbling process of the CubeSat. The second component is the filters that separate the transmitter from the receiver. The two filters have high roll off and narrow fractional bandwidth within a compact area. The transceiver system is based on the analog devices chip AD9361 controlled by zynq-7000 FPGA. The output RF signal is amplified to approach 33dBm output power to the antenna port via QORVO chip that operates in the range from 700MHz to 2700MHz. The antennas and filters are fabricated and tested where good results are noticed so that they are ready for integrating with the whole CubeSat communication subsystem.

INDEX TERMS CubeSat, S-band antenna, hairpin filter, transceiver system, FPGA, and satellite.

I. INTRODUCTION

With the advent of the new millennium, the world witnessed a boom in satellite missions that served different applications such as atmospheric science, telecommunications, monitoring the weather and so many applications [1].

It was evident from the many missions of small satellites, called micro-, nano-, and pico-satellites, that was recently launched side by side with the huge geostationary orbit (GEO) or the classical big medium earth orbit (MEO) and low earth orbit (LEO) satellites that it will take more place in the current and near future.

The associate editor coordinating the review of this manuscript and approving it for publication was Hassan Tariq Chattha.

The use of a network of tens of small satellites compared to large satellites has several features such as their light-weight, low volume, low communication latency, low cost and, high fault tolerance [2].

The challenging task in the design of small satellites is the capability of miniaturizing the different electronics components and subsystems [1]. This is already existing with the appearance of systems on chips technologies, miniaturized antenna and filter designs, battery systems with high capacity and small size, etc. [3].

The most popular nanosatellites are CubeSats [4]. The standard dimensions of one unit (1U) of CubeSat are (10 × 10× 10 cm). CubeSat has different configurations according to the number of cubic units that constitute it. It may be 2U, 3U.... or 6U. Each unit (U) has the standard dimensions

This work is licensed under a Creative Commons Attribution 4.0 License. For more information, see https://creativecommons.org/licenses/by/4.0/

($10 \times 10 \times 10$ cm). The software-defined radio SDR system is already fitted within IU of the CubeSat while the remaining units may be used for different Payloads and other instruments necessary for their satellite's functionality.

The CubeSats operates in the VHF, UHF, L, S, X, Ka, and V bands [5]. 50% of the power consumed by the CubeSats is for the communication subsystems which may last a few times per day when the satellite is in line of sight with the ground station.

The communication link between the CubeSat, and the ground station cannot be established properly without the good design of the antenna. The antenna design should fulfill the CubeSat standards [6] such as the size, and multifunctional capabilities. The design should deal carefully with the trade-off between the antenna size, and its parameters such as the gain, and radiation pattern.

The categories of the used CubeSat antennas as stated in literature [7] are; wire antennas in the UHF/VHF bands, reflector antennas operating from S-band to Ka-band, and reflectarrays operating at X-band and Ka-band. Other configurations such as the membrane antennas, planar antennas, and horn, and guided wave antennas are also utilized for the CubeSats.

In most compact systems such as mobile systems, CubeSat, and other commercial applications, planar antennas have superiority over other configurations due to their low profile and relative ease of fabrication. A good survey regarding the use of planar antennas in CubeSats is reported in [8]. In [9]–[12], meshed, and transparent antennas are utilized in CubeSats. In [13], an S-band patch antenna array is investigated. On the other side, the inverted F planar array is proposed in the S-band communication for the CubeSat [14] and [15].

In this study, the S-band antenna design is one of the main targets. Extensive studies regarding this type of antennas are investigated in literature [16]–[24].

In [16], [17], a four patches antenna is designed to radiate at a center frequency of 2.45 GHz. A Wilkinson power divider is placed in another layer underneath the antenna layer. This antenna can operate with linear polarization or circular polarization. The antenna polarization can be modified according to the phase difference between each antenna element. In [18], a patch antenna fed by a 3-dB coupler is used. This antenna operates at L-Band and S-Band with a bandwidth equals to 0.535 GHz, and 0.275 GHz, respectively. This antenna structure provides good performance but also hard to implement. In [19], an antenna with parasitic elements around the main radiator is introduced. The overall structure is composed of the main radiator of two crossed bowtie-shaped dipole antennas, and a feeding network using a Wilkinson power divider with phase difference between two parts to provide circular polarization. In [20], a patch antenna with two slotted corners is introduced. A coaxial probe is used to feed the antenna. This antenna provides a good gain that equals to 7 dBic but with a narrow axial ratio bandwidth which only covers 25 MHz. In [21], four dipole antennas with a phase delay line are introduced. This antenna provides a good performance in the operating bandwidth. The need for a reflector to minimize the back radiation increases the antenna height. In [22], a steerable Yagi-Uda antenna implemented on a dielectric is proposed. The antenna consists of 3 elements lying on an FR4 substrate that forms an angle with the CubeSat's surface. The antenna provides a high gain equal to 8 dBic with linear polarization. In [23], a high gain coplanar waveguide (CPW)–fed slot antenna with a metasurface superstrate structure (MSS) is introduced. The use of MSS significantly improves gain, and reduces back-lobe radiation. The antenna achieves a bandwidth (BW) of 1.37 GHz and a gain of 8.8 dBic. The use of MSS, and reflector increases the antenna height. In [24], An F-shaped patch antenna is proposed for CubeSats communications. The use of two arms with different lengths generates a second resonant frequency to increase the bandwidth. The antenna structure makes it not suitable for vibrations.

The challenge is to design two separate circularly polarized antennas, and fit in the available space in the CubeSat face. It is also necessary to provide a low mutual coupling between the two antennas with suitable bandwidth, and wide beamwidth.

Moreover, improved performance, and reduced size Tx/Rx filters are urgently needed for uplink / downlink signal separation. Hairpin BPF approach [25]–[26] is selected to be employed in the filter design procedure. Two BPF filters are designed, optimized, fabricated, and tested. The proposed filters meet the project standards well.

The contributions in this paper are summarized as follows:

1. Propose a reliable CubeSat subsystem that take the tumbling problem after launching into considerations.
2. Design and fabricate a reliable antenna system that meet the required specification comparing results with literatures.
3. Design and fabricate reliable filters that separates the uplink from the downlink with minimum size and minimum losses comparing results with literatures.
4. Propose the remaining system components with proper selection of its characteristics and positions

II. COMMUNICATION SYSTEM CONSTRUCTION

Our system specifications, described in Table 1, require the separation of the Tx band and Rx band.

Fig. 1 illustrates the block diagram of the proposed CubeSat communication system. It consists of 4 basic boards: 2 antenna boards, FPGA board, RF board, and power amplifier, power dividers, and filters board. Each antenna board consists of two circularly polarized antennas; one of them is used as a receiver in the band (2.025 GHz to 2.11 GHz), and the other acts as a transmitter in the band (2.2 GHz to 2.29 GHz). The antenna boards are placed in both the front, and bottom faces of the CubeSat to get a very wide HPBW. This structure is required to establish the first communication with the ground station. The primary antenna located in the front face is used to establish reliable communication with the

TABLE 1. The required system specification of our CubeSat mission.

Spec.		Required Value
Frequency	Up Link	2.025 GHz: 2.11 GHz
	Down Link	2.2 GHz: 2.29 GHz
Input impedance		50 ohm
VSWR		< 1.25
Front to back ratio F/B		> 15 dB
Gain		>3 dBic
Polarization		left-hand circular polarization (LHCP)
Beam Width	Vertical	$\pm 35^{o} \pm 5^{o}$
	Horizontal	$\pm 35^{o} \pm 5^{o}$
Weight		< 50 g
Power	Tx	2W
	Rx	-110dBm
Dimensions		10cm * 10cm

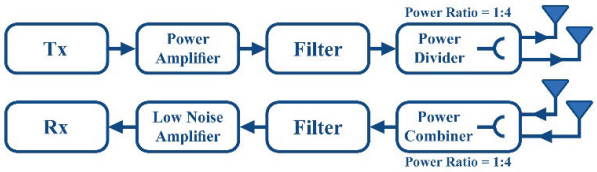

FIGURE 1. Block diagram of the S-band transceiver board.

ground station. The secondary antenna that is in the bottom face is used for navigating the satellite to its right position.

Due to the tumbling process after lunching; the CubeSat will alter its position and orientation several times. This tumbling makes the antenna to face the earth station for short time. This may cause loss of communications for long time. In order to mitigate this event, two sets of antennas in opposite directions are placed on the body of CubeSat. The power is divided between the two antennas by 1:3. The link budget is calculated according to the lowest transmitted power. Although the Bit Error Rate (BER) increases with the decreasing of the power in the back direction, successful link budget is still existing.

Moreover, The CubeSat has six faces, if the antenna is in one face only, the probability of successful communication during the tumbling process may be a sextant, but if two sets of antennas on opposite directions are used the probability will be doubled. So, the use of two sets of antennas will enhance the communication between the CubeSat and the earth station, and decrease the probability of communication interruption.

Fig. 2 depicts a 3D model for the proposed S-band CubeSat communication subsystems structure illustrating the position, and the relationship of each board with its contiguous boards.

In the following section, the antenna design, and configuration are explained in detail with its results, and discussions. In section IV, the filter design is illustrated with detailed results and discussions. Other boards are briefly explained in section V. Finally, the conclusion is introduced in section VI.

III. ANTENNA DESIGN AND CONFIGURATION

A. ANTENNA GEOMETRY

The proposed antenna consists of two circularly polarized square patches; the smaller one is for the downlink band and the other one for the uplink band as shown in Fig. 3.

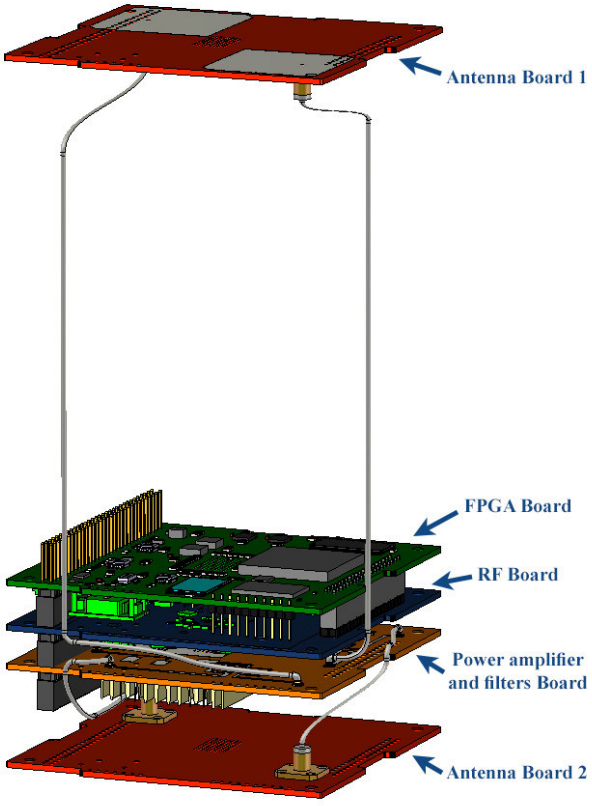

FIGURE 2. The 3D configuration of the S-band transceiver board.

The use of two separate antennas for transmitting and receiving instead of one multi-band or wideband antenna for both Tx and Rx is to keep the Tx /Rx antenna system as simple as possible. If we choose monostatic approach (i.e., one antenna for both Tx / Rx paths), a complicated switching circuit should be added. The switching circuit will add losses. Moreover, extra weight will be added to the CubeSat. So, the use of two separate antennas is considered the most suitable solution in this case.

For circular polarization radiation, a patch must support orthogonal fields of equal magnitude but in-phase quadrature. Each patch is fed by two feed points which are chosen perpendicular to each other to excite two orthogonal modes. Here the two probes are fed through a Wilkinson power divider, with one arm of the output feed lines a quarter-wavelength longer than the other to produce a 90^{o} phase shift as shown in Fig. 4.

The antenna feeding system is based on two identical Wilkinson power dividers, as shown in Fig. 4. The power divider arm's length (L_{p70}) is chosen initially to be quarter wave of the guided wavelength ($\lambda_g/4$) with characteristic impedance of 70.7 ohms. Moreover, 100 ohms surface mounted resistance is connected between the power divider arms, in order to enhance the output ports isolation. The optimized dimension of the feeding structure is tabulated in Table (2).

The Wilkinson power divider can be modeled as a junction of three transmission lines [27] as shown in Fig. 5. In general,

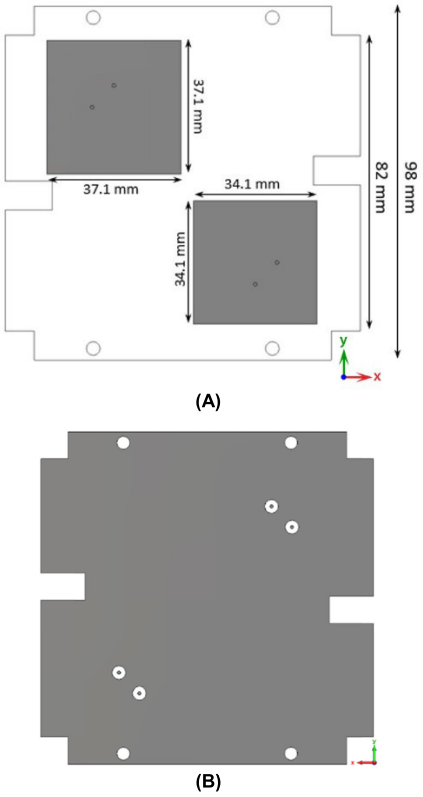

FIGURE 3. Structure of the proposed antenna. (A) front view, (B) back view.

TABLE 2. The optimized dimensions of the antenna feeding system.

Parameter	L_{p70}	W_{p50}	L_{pf}	W_{p70}	D_o	D_{in}
Value in mm	23.015	1.11	17	0.56	4	1

there are fringing fields and higher order modes associated with the discontinuity at such junction leading to stored energy that can be accounted for by a lumped susceptance, B. However, if we consider the transmission lines to be lossless then the lines characteristic impedances will be real and the lumped susceptance, B will be zero. In order to achieve good matching, the input admittance of the input port should be following Eq. 1.

$$Y_{in} = \frac{1}{Z_o} = jB + \frac{1}{Z_1} + \frac{1}{Z_2} \approx \frac{1}{Z_1} + \frac{1}{Z_2} \tag{1}$$

where, $Z_1 = Z_2 = \sqrt{2}\, Z_o$ to achieve equal power division and full input port matching, and $Z_S = 2Z_o$ to achieve output ports isolation. Where Z_o is the characteristic impedance of both input and output lines of the power divider.

The S-parameters of the ideal 2-way equal-split Wilkinson power divider at the design frequency can be obtained from [27] as:

$$[S] = \frac{j}{\sqrt{2}} \begin{bmatrix} 001 \\ 100 \\ 100 \end{bmatrix} \tag{2}$$

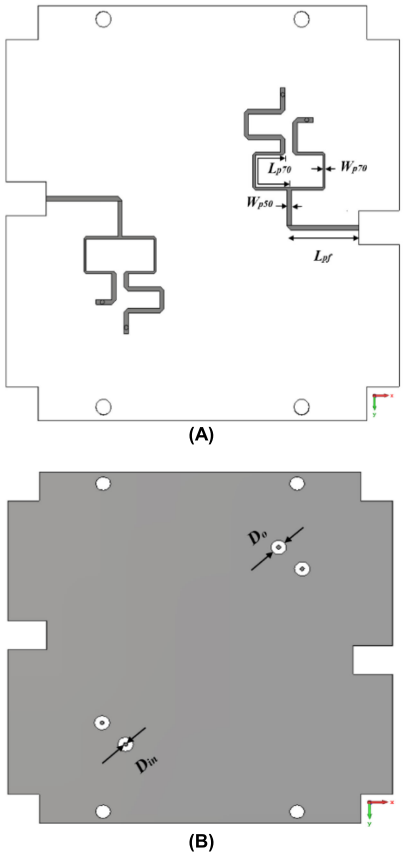

FIGURE 4. The feeding structure of the proposed antenna. (A) front view, (B) back view.

Investigating the S-matrix shows that the ideal network is reciprocal ($S_{ij} = S_{ji}$), that the terminals are matched ($S_{11} = S_{22} = S_{33} = 0$), and that equal power division is achieved ($S_{21} = S_{31} = -3dB$).

Complete odd-even mode analysis of Wilkinson power divider is provided in [27]. In order to take the practical case, full wave analysis using the CST software is introduced.

The proposed antenna is printed on a low-loss dielectric substrate Rogers RO4003C with a dielectric constant of $\varepsilon_r = 3.38$, substrate height (h) = 1.524 mm, and loss tangent 0.0027 which has high-reliability characteristics for aerospace applications. However, the feeding network is fabricated on RO4350B substrate which has a dielectric constant of $\varepsilon_r = 3.48$, substrate height (h) = 0.508 mm, and loss tangent of 0.0037. The dimensions of the antenna are positioned on Fig. 3 (A) while that of the feeding structure are tabulated in Table 3.

With such a substrate, the dimensions of the two patches are calculated then optimized to have one antenna operating in the downlink band, and other antenna operating in the uplink band. The dimensions of the transmitter antenna and the receiver antenna are 34.1 x 34.1 mm^2 and 37.1 x 37.1 mm^2, respectively. In order to achieve the best matching, it has been found from the simulations that the two feeding points of the single patch have to be placed 6 mm away

TABLE 3. The antenna comparison table.

Ref.		Size (mm3)	f_0 (GHz)	BW (GHz)	AR BW (GHz)	HPBW (°)	Gain	Polarization
[16]		96 x 96 x 2.1	2.45	-	-	45	3.7 dBi	LP
[17]		96 x 96 x 2.1	2.45	-	-	60	7.3 dBic	CP
[18]		100x100x14.75	1.62 2.5	1.33-1.89 (0.535) 2.36-2.64 (0.275)	1.53-1.69 (0.16) 2.45-2.55 (0.1)	-	8.5 dBic 8.2 dBic	CP
[19]		-	2.16	2.025-2.29 (0.265)	2.025-2.29 (0.265)	85	7.6 dBic	CP
[20]		46.683x46.683 x1.58	2.4	2.37-2.43 (0.06)	2.39-2.415 (0.025)	-	7 dBic	CP
[21]		55x55x0.85	2.4	2.05-2.87 (0.82)	2.26-2.53 (0.27)	-	3.49 dBic	CP
[22]		-	2.45	2.3-2.55 (0.25)	-	-	8.877 dBic	LP
[23]		90x90x10.5	2.45	1.6-2.97 (1.37)	2.34-2.47 (0.13)	-	9.71 dBic	CP
[24]		33.8x88.4x18.4	2.45	1.606-2.727 (1.121)	-	98.43	8.51 dBic	-
[25]	Planar	100 x 100 x 0.5	5.8	5-7 (2)	-	-	7.5 dBi	LP
	Folded	32.5x32.5x 32.5	5.8	5-7 (2)	5-6 (1)	60	10 dBic	CP
[26]		78x75x19.6	2	2-2.45 (0.45)	1.9-2.45	70	3 dBic	CP
Proposed (Rx Antenna)		38.5*43.5*2.1	2.0675	2.025-2.116 (0.088)	2-2.154 (0.154)	78	5.5 dBic	CP
Proposed (Tx Antenna)		36*43*2.1	2.245	2.188-2.3 (0.112)	2.2-2.305 (0.105)	77	5 dBic	CP

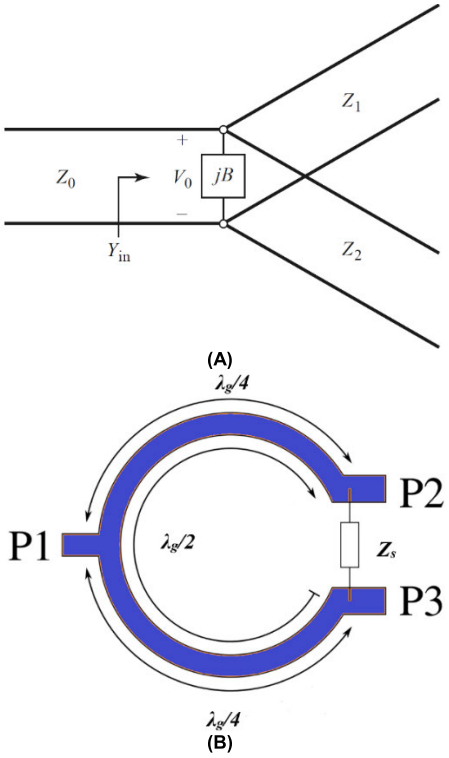

FIGURE 5. Transmission line model for Wilkinson power divider. (a) the equivalent circuit of input T-junction of the power divider [27], (b) the full model of Wilkinson power divider.

from the antenna center. The final antenna system was then achieved by assembling the two Rogers substrates in a single structure. This has been done by connecting together the two ground planes using electrically conductive glue and connecting the feed-line terminations to the patch feed-point with metallic pins inserted in the via-holes. The layer stack-up of the designed antenna is shown in Fig. 6.

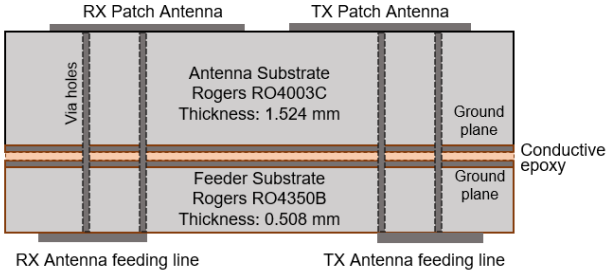

FIGURE 6. Layer stack-up of the designed antenna.

The total antenna design can be fitted in 80 x 80 mm^2 square board, which is suitable for the space available for the antenna on the top, and bottom faces of the CubeSat.

B. ANTENNA RESULTS AND DISCUSSION

The proposed antenna is simulated using a Computer Simulation Technology (CST), ver. 2019.

To verify the simulations, the antenna, and the feeding network are fabricated using the photolithographic technology on RO4003C, and RO4350B substrates, respectively. The S-parameters are measured using Vector Network Analyzer (VNA) ZAV67 after the standard calibration procedure. Fig. 7 (a) shows the practical setup for the antenna measurements where the radiating face appears in the figure. Fig.7 (b) illustrates the feeding network beneath the substrate of the radiating elements.

Fig. 8 presents the simulated S-parameters of the feeding network. It is shown that the magnitude bandwidth is wide enough to include both the uplink and downlink bands as shown in Fig. 8 (a). Similarly, the phase shift between the two feeding points of each antenna approaches 90° withing the operating bands for both the transmitting and receiving

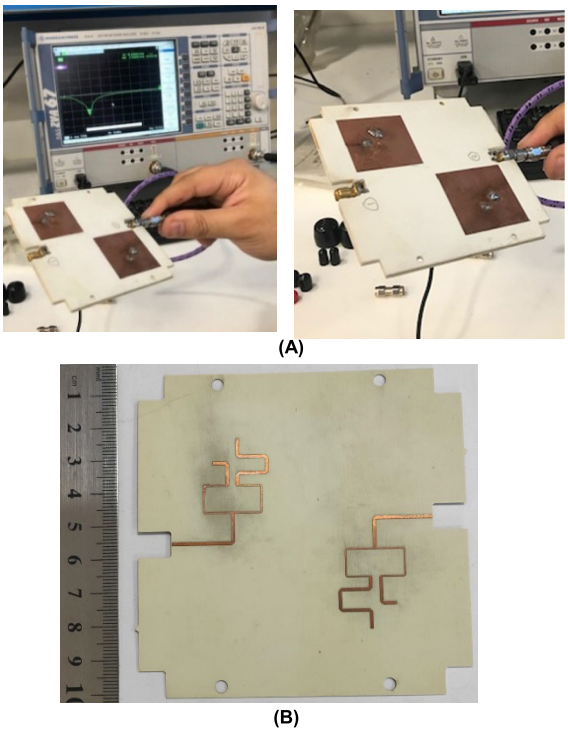

FIGURE 7. Practical setup for the antenna measurement (a) Tx/Rx antennas (b) feeding networks (Wilkinson power dividers).

antennas to guarantee circularly polarized radiations as shown in Fig. 8 (b).

Fig. 9 shows both the simulated, and measured reflection coefficients $|S_{11}|$ of the receiver antenna, and $|S_{22}|$ of the transmitter antenna. It is depicted from Fig. 9 that the practically designed antenna covers the required operating bandwidth that extends from 2.025 GHz to 2.116 GHz for the receiver antenna, and from 2.188 GHz to 2.3 GHz for the transmitter antenna. Fig. 10 shows the measured, and simulated results of the isolation $|S_{21}|$, and $|S_{12}|$ between the two antennas where it is noted that the isolation between the two elements is better than -35 dB. $|S_{21}|$ is > -35 at the upper end.

The antennas show good performance with a frequency shift of 12 MHz for the Rx antenna, and a frequency shift of 8 MHz for the Tx antenna, as shown in Fig. 9. This can be accounted to the substrate material variation in its permittivity, and to the soldering of the connectors.

To further verify the field pattern at the selected resonant frequency for the proposed antenna, the antenna is measured using the Satimo StarLab setup as shown in Fig. 11.

Fig.12 illustrates the maximum gain of the transmitting and receiving antennas in the broadside directions. The gain of the Rx and Tx antenna were recorded at 2.0675 GHz and at 2.245 GHz, respectively to be 5.5 dBic. Good performance of both antennas is noticed.

The Axial ratio is a measure for the ratio between the two orthogonal components of the electric fields emanating from the antenna. Its ideal value is 0 dB but practically the antenna is conventionally categorized as a circularly

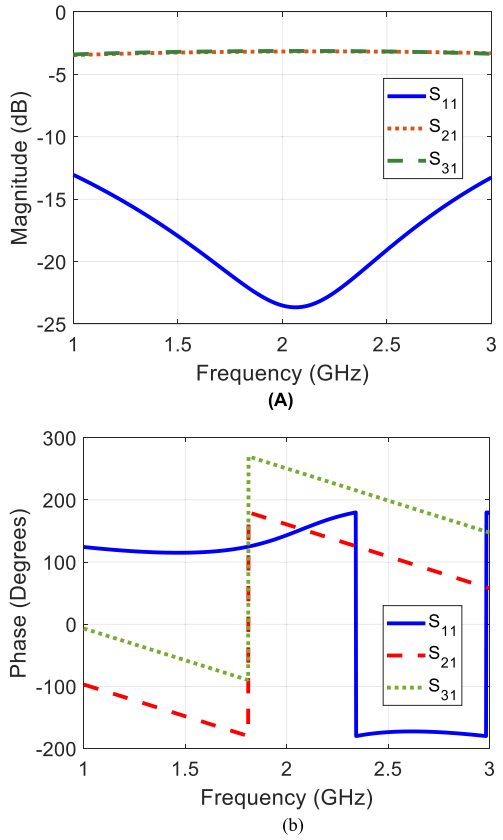

FIGURE 8. S-parameters for the feeding networks (Wilkinson power dividers). (a) Magnitude (b) Phase.

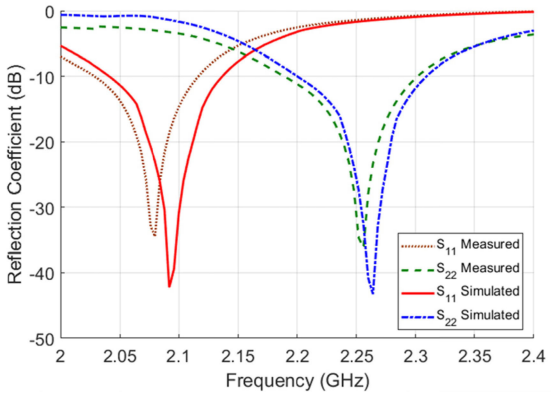

FIGURE 9. S-parameters of the proposed antennas, simulated, and measured.

polarized antenna if the axial ratio deviation does not exceed 3 dB within a certain frequency band or certain radiation angles [10]–[12].

Fig. 13 illustrates a comparison between the measured, and the simulated axial ratio of the two antennas in the required frequency bands. It is noticed that the axial ratio of both antennas is less than 3 dB along with both bands (2.025 GHz - 2.11GHz), and (2.2 GHz to 2.29 GHz).

The normalized radiation patterns of the receiving and transmitting antennas are illustrated in Fig. 14 and

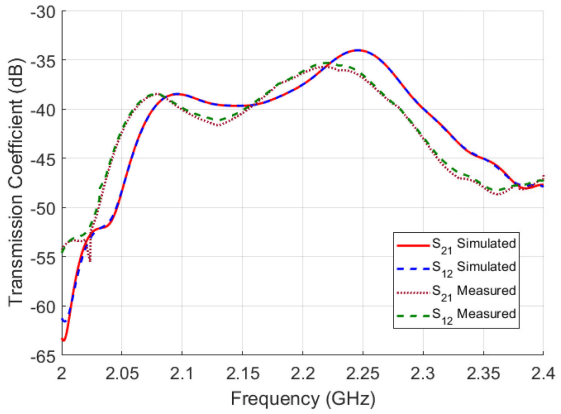

FIGURE 10. Simulated, and measured results of the isolation $|S_{21}|$, and $|S_{12}|$ between TX antenna, and RX antenna.

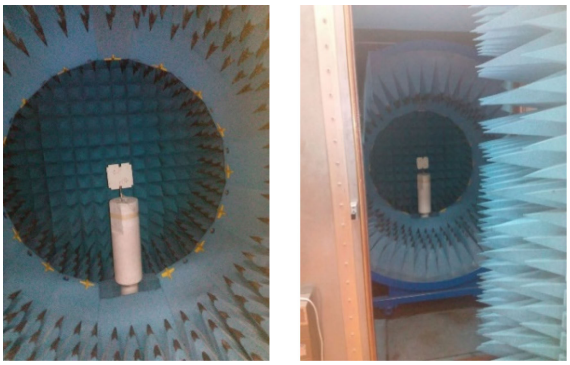

FIGURE 11. Practical setup for Tx antenna radiation pattern measurement.

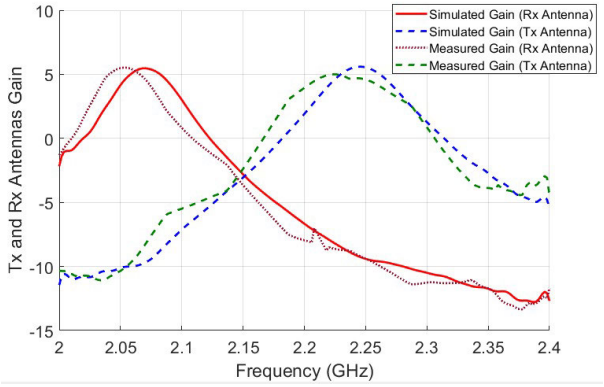

FIGURE 12. The gain of the two antennas.

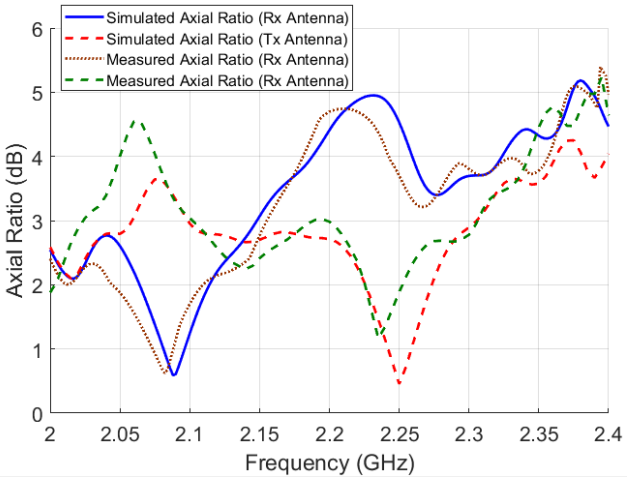

FIGURE 13. The axial ratio of the two antennas against frequency.

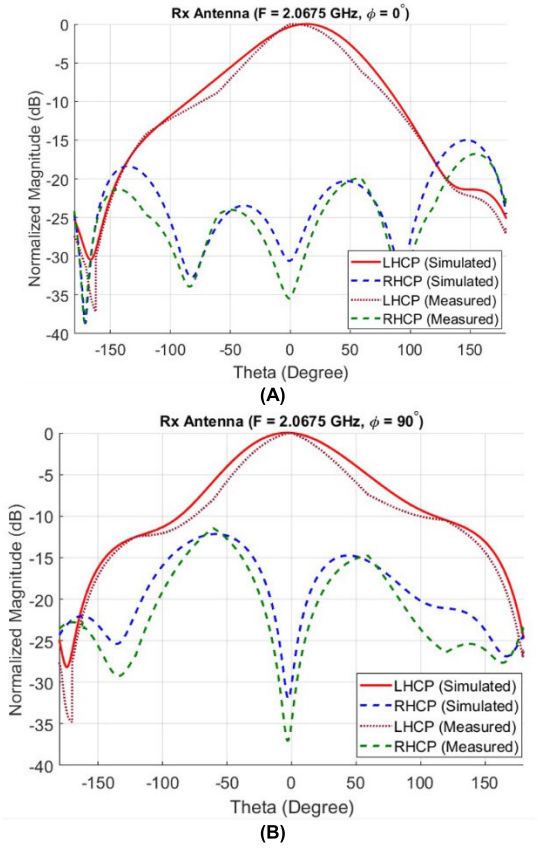

FIGURE 14. Simulated, and Measured results of radiation pattern (Cartesian) of RX antenna at uplink center frequency. (A) $\Phi = 0^{o}$, (B) $\Phi = 90^{o}$.

Fig. 15, respectively in Cartesian coordinates. It is shown from the figures that the desired LHCP field component exhibits a wide beamwidth and a high degree of rotational symmetry.

Fig. 14, and Fig. 15 illustrates that the cross-polar RHCP component is quite weak. The figures show that the measured HPBW is around 78^{o} for both the Rx antenna and the Tx antenna at the two planes. The cross-polarization discrimination (XPD) level is measured within the beam width to be 14 dB, and 15 dB for the Rx antenna, and Tx antenna, respectively. The direction of maximum radiation is observed to be in the broadside direction ($\theta = 0^{o}$).

Table 3 illustrates a comparison between the proposed CubeSat antenna and the other antennas in recent literature [16]–[24] related to S-band CubeSat communications. The antenna satisfies the system requirements in Table 1; the size of the antennas and its HPBW lies within the accepted

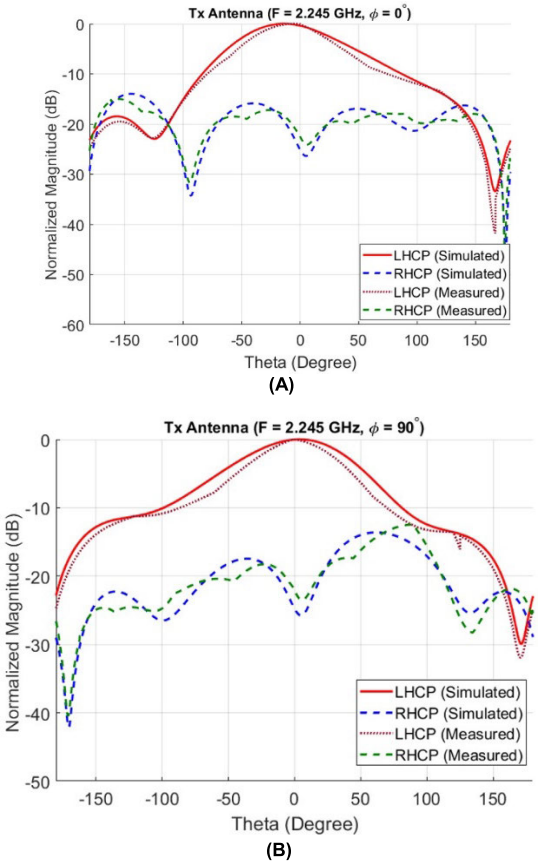

FIGURE 15. Simulated, and Measured results of radiation pattern (Cartesian) of RX antenna at uplink center frequency. (A) $\Phi = 0^{o}$, (B) $\Phi = 90^{o}$.

range as listed in Table 1, the F/B approaches 17 dB, more than 5 dBic gain, and LHCP with XPD of 14 dB within the operating band.

The proposed design can be considered as a compromised solution offering proper performance, and keeping the size parameters of the project. For example, the proposed antenna achieves circularly polarized gain of 5.5 dBic, when it is compared to the published references introduced in Table 4, one can find that this value is smaller than [17], [18], [22], [24], [25]. However, on the other hand the areas of these antennas are much larger than ours. In this project, we have an antenna size restriction to keep its size within 10 Cm x 10 Cm. In terms of HPBW, and concerning reference [17], [25], and [26], one can find that our design beamwidth is larger than them which means broader coverage to the earth station.

IV. FILTER DESIGN AND IMPLEMENTATIONS

Bandpass filters play a significant role in the CubeSat wireless communication system. Uplink, and down-link signals have to be filtered at a certain center frequency with a specific bandwidth. Bandpass filters (BPF) with improved out of band performance, reduced size, and high spurious band rejection are required in modern RF, and microwave communication systems. BPF designed using split-ring resonators

TABLE 4. Tx and Rx Filter Specifications.

	Tx Filter (downlink)	Rx Filter (uplink)
Operating frequency	2.2 GHz-2.29 GHz	2.025 GHz-2.11 GHz
Filter model	0.1 dB Chebyshev	0.1 dB Chebyshev
Filter order	3	3
FBW % (Δ)	0.05537	0.05537
Bandwidth	125 MHz	125 MHz
Center Frequency	2.2575 GHz	2.0625 GHz

has relatively large circuit losses, while BPF using parallel coupled-lines has a large size, and poor selectivity [28]. Hairpin-line bandpass filters are compact structures [29]. These are widely used at lower microwave frequencies where compactness is desirable for coupled lines. The design of Hairpin-line bandpass filters has been investigated widely in literature [29], [30].

According to the selected operating frequency bands for both the transmitter and the receiver in this project, the specifications tabulated in Table 1 are deduced to separate the transmitter signals from the receiver signals.

Hairpin filter is the most popular and widely used configuration in microstrip band pass filters due to their compact design and ease of fabrication using microstrip technology. They are conceptually obtained by folding the arms of normal parallel coupled $\lambda/2$ resonators into U shape to reduce the size of filter. Hence, same design equations for parallel coupled half wavelength resonators can be used. However, to fold the resonators it is necessary to take into account the reduction of the coupled-line lengths, which reduces the coupling between the resonators. The line between two bends tends to shorten the physical lengths of the coupling sections, and the coupled section is slightly less than a quarter wavelength.

The challenging task is to design two hairpin filters; one for the transmitter, and the other for the receiver where the size of the two filters should fit the available space in the board as well as choosing the optimum filters order that allow the separation between the uplink, and downlink bands especially with the very narrow guard gap between the two bands.

In the filters design, and implementation, the following steps of design are followed;

1. Propose a lumped element model for an LPF.
2. Lumped elements LPF conversion to BPF
3. Lumped elements conversion to Hairpin coupled lines
4. Full wave simulation and parameters optimization
5. Fabrication and testing of the Filters
6. Adjusting Filter parameters and refabricating and testing Filters

A. PROPOSE A LUMPED ELEMENT MODEL FOR AN LPF

The design started with the selection of prototype elements from the Chebyshev 0.1 dB ripple factor for the low pass filter

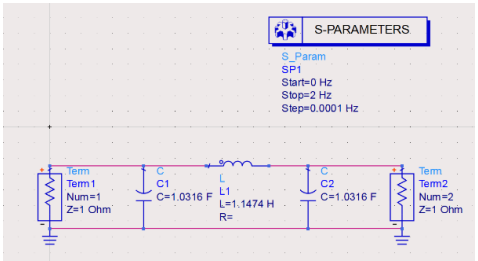

FIGURE 16. Schematic diagram of LPF model, n = 3.

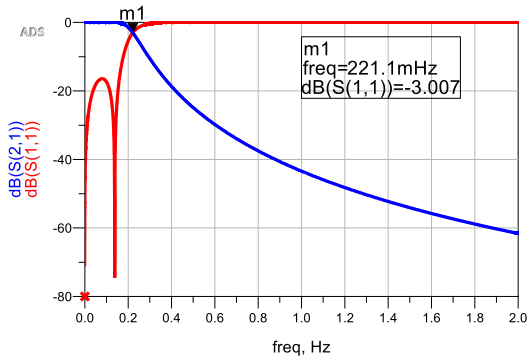

FIGURE 17. S-parameters of the simulated LPF model.

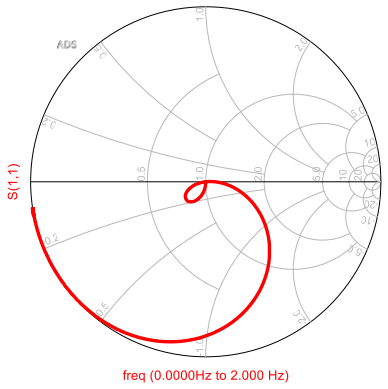

FIGURE 18. Reflection coefficient S11 of the simulated LPF model.

model [29]. The reason for that is to reduce the ripples in the passband and to increase the filter roll-off. The full electrical specifications of the proposed Tx and Rx filters are tabulated in Table 4.

In order to test our design procedure, the LPF circuit model is simulated using ADS 2019 software package, where its schematic diagram is shown in Fig. 16. The simulated results of the ideal LPF model, shown in Fig. 17, indicates that the −3dB cutoff frequency occurs at 0.221 Hz. Filter reflection coefficient S_{11} shows good matching level over the passband as illustrated in Fig. 18. It is worth remembering that low pass prototype elements are normalized for a Cutoff frequency of 1 Radian per second, and source & load resistance of 1Ω.

B. LUMPED ELEMENTS LPF CONVERSION TO BPF

The low pass prototype elements are converted to bandpass configuration using formulas listed in [29]. Impedance and

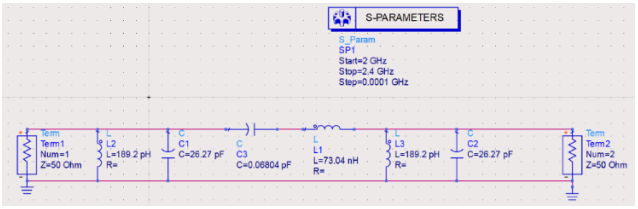

FIGURE 19. Schematic diagram of the scaled BPF model (Tx Filter).

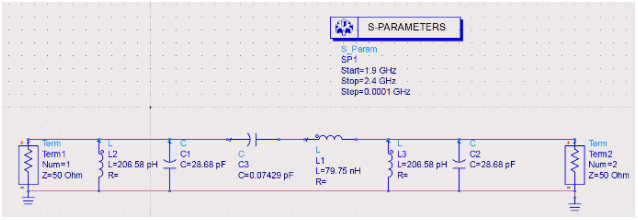

FIGURE 20. Schematic diagram of the scaled BPF model (Rx Filter).

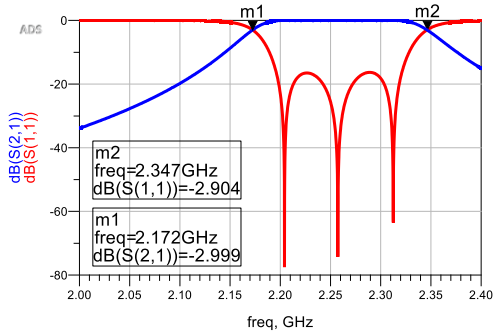

FIGURE 21. S-parameters of the scaled BPF model (Tx Filter).

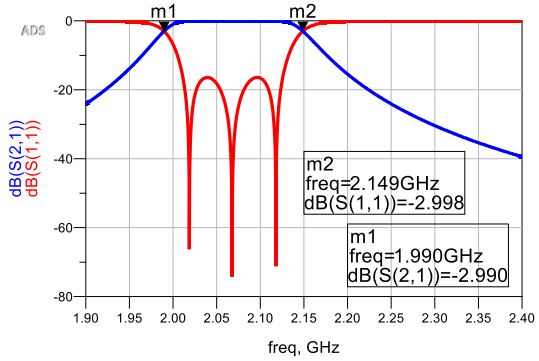

FIGURE 22. S-parameters of the scaled BPF model (Rx Filter).

frequency scaling are also being done in the same step using the same formulas. The schematic diagram of the transmitter and receiver filters are illustrated in Fig. 19 and Fig. 20, respectively. The S-parameters of the Tx filter are shown in Fig. 21 while the S-parameters of the Rx filter is shown in Fig. 22. It can be noticed that the passband (−3dB BW) of the proposed Tx filter is located over the range from 2.172 GHz up to 2.172 GHz, which makes it fully covering the required band in the specifications. Moreover, the Rx filter satisfies the operating band too, where its operating band ranges from 1.99 GHz to 2.14 GHz.

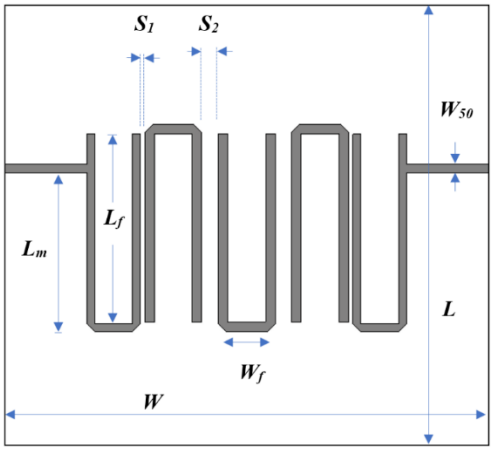

FIGURE 23. The schematic diagram of the proposed Tx, and Rx filters.

TABLE 5. The optimized dimensions of the proposed Tx filter.

Parameter	Value in mm
L_m	9.76
L_f	11.594
S_1	0.2706
S_2	1.01219
W_f	2.3149
W	29.5
L	20
W_{50}	0.52

TABLE 6. The optimized dimensions of the proposed Rx filter.

Parameter	Value in mm
L_m	9.744
L_f	12.594
S_1	0.274
S_2	1.0138
W_f	2.3149
W	29.23
L	20
W_{50}	0.52

C. CONVERSION TO HAIRPIN CONFIGURATION USING MICROSTRIP TECHNOLOGY

Fig. 23 shows the geometry of the proposed Tx/Rx filters. The U-shaped sections of the hairpin filter are printed on a high permittivity "$\varepsilon_r = 10.2$" substrate (RT6010) with a metal thickness t = 0.035 mm, dielectric thickness h = 0.635 mm, and tangential loss of 0.0023. Choosing this substrate can be accounted for two reasons, the first one is to make the EM wave confined inside the substrate, and to reduce the unintentional radiation, while the second reason is due to its compatibility to the satellite applications. The design parameters are calculated based on formulas in [29]. The Tx, and Rx dimensions are tabulated in both Table 5, and Table 6, respectively.

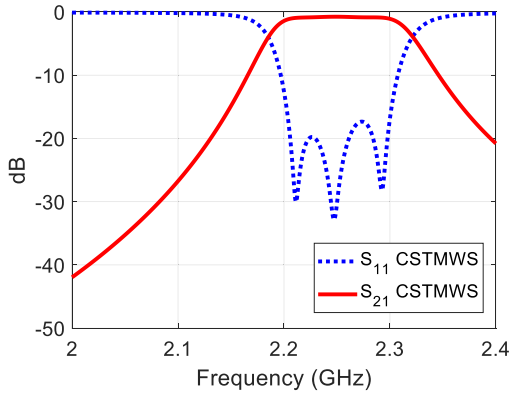

FIGURE 24. S-parameters of the proposed Tx hairpin filter (simulation).

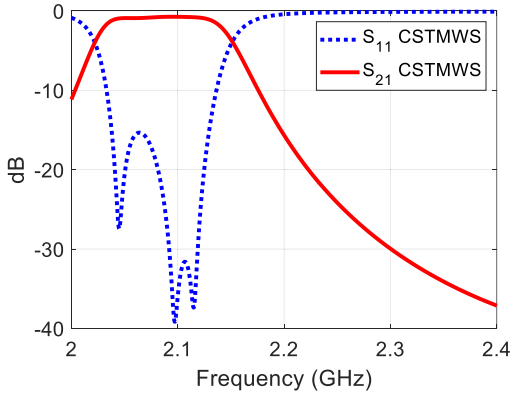

FIGURE 25. S-parameters of the proposed Rx hairpin filter (simulation).

D. FULL WAVE SIMULATION, AND PARAMETERS OPTIMIZATION

For design verification, the proposed filters (Both Tx, and Rx) are simulated using Microwave Studio CSTMWS 2019 software package. Besides, for more accuracy assurance, a frequency domain solver is adopted.

Both Fig. 24, and Fig. 25 show the S-parameters of the optimized Tx, and Rx filters, respectively. It can be noticed that the insertion loss of both filters is 0.9 dB (max.), and superior matching performance is obtained (less than −15 dB) in the range of 2.2 GHz−2.3 GHz for the Tx filter, and 2.04 GHz- 2.11 GHz for the Rx filter.

Fig. 26, and Fig. 27 illustrate the surface current distribution for the proposed Tx filter. It can be noticed clearly that the EM wave cannot pass at the stop band (i.e., at 2.06 GHz), however, it can easily pass through the filter at 2.25 GHz.

On the other hand, Fig. 28, and Fig. 29 show that the EM wave cannot propagate through the Rx filter around 2.25 GHz, while it can pass smoothly at 2.06 GHz (mid of its passband).

E. PRACTICAL MEASUREMENTS

In order to verify the simulations, The Tx filter is fabricated using the photolithographic technology on RT 6010 substrate. The filter is fitted in the Anrtisu test-in fixture, then its S-parameters are measured using Vector Network

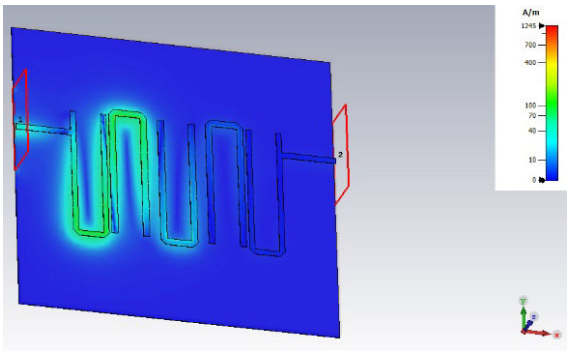

FIGURE 26. Surface current distribution for the Tx filter at 2.06 GHz.

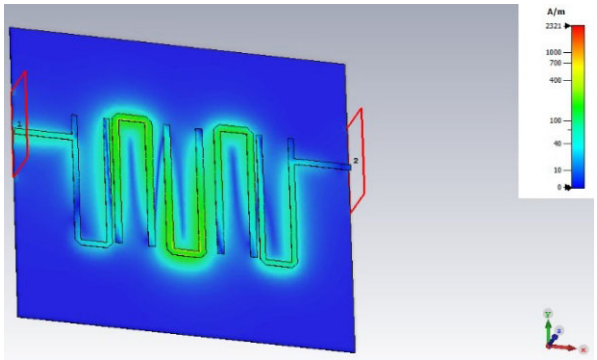

FIGURE 27. Surface current distribution for the Tx filter at 2.25 GHz.

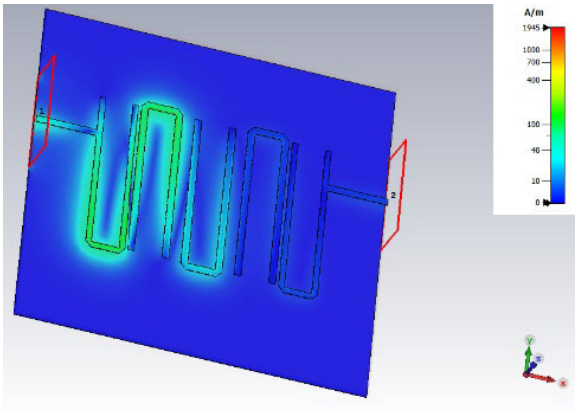

FIGURE 28. Surface current distribution for the Rx filter at 2.25 GHz.

Analyzer (VNA) ZAV67 after standard calibration procedure. Fig. 30 shows the measurement setup.

The filter shows good performance with a frequency shift of 57 MHz for the passband (2.143 GHz to 2.243 GHz), as shown in Fig. 31. This can be accounted to the substrate material variation in its permittivity, where the datasheet's permittivity value is usually recorded at 10 GHz. Furthermore, the passband insertion loss (S_{21}) of the filter is found to be around 2 dB, which is higher than the simulated one by 1.1 dB. This increase in losses can be accounted for the port losses of the test-in fixture. Table 7 illustrates the comparison between the proposed design and other designs published in literatures.

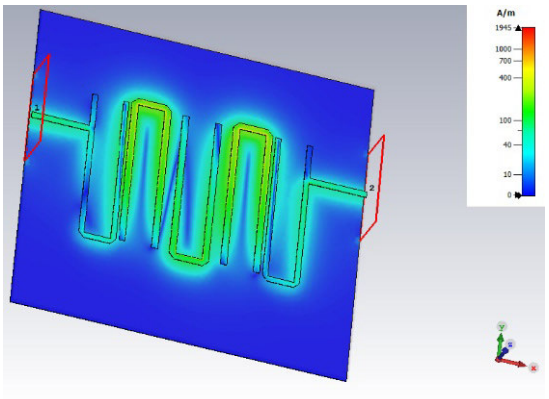

FIGURE 29. Surface current distribution for the Rx filter at 2.06 GHz.

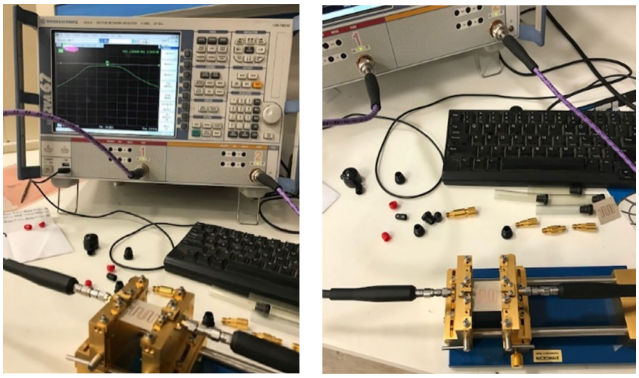

FIGURE 30. Practical setup for Tx hairpin filter measurement using test-in fixture.

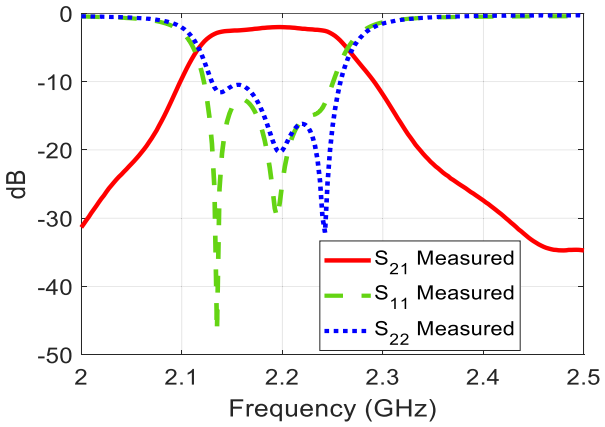

FIGURE 31. S-parameters of the proposed Tx hairpin filter (Experimental).

F. FINAL OPTIMIZATION, AND FINE TUNING

As the experimental results indicate that the proposed Tx filter design suffers from an obvious frequency shift of 57 MHz, corrected versions of the two filters (Tx and Rx) should be designed, fabricated, then tested.

Both Table 8, and 9 represent the corrected dimensions of the Tx, and Rx filters. Photo of the final Tx and Rx filters are shown in Fig. 32, and Fig. 33, respectively.

Fig. 34, and Fig. 35 shows the experimental results of the filters after dimension corrections. It can be noticed that both Tx, and Rx filters achieve the required specifications.

TABLE 7. The Filters comparison table.

	Size in mm	Operating B.W.	FBW	Max. Insertion loss	Roll off in the rejection band	Order	Type
[31]	120 mm * 80 mm	3.05–3.96 GHz	0.285	0.25 dB	613 dB/Decade	3rd order	N.A.
[32]	120 mm * 42.5 mm	225-400 MHz (three switchable sub-bands)	2.5 – 2.6	9.2 dB	1649 dB/Decade	4th order	N.A.
[33]	LPF with cutoff frequency fc at 3 GHz implemented on a 0.5-mm-thick MgO wafer. It has a 30-dB harmonic suppression from 1.08 fc to 7 fc, a steep roll-off of 197.1 dB/GHz, and an in-band insertion loss less than 0.13 dB.						
[34]	30 mm * 25 mm	0.9- 1.1 GHz	0.2	1.5 dB	550 dB/ Decade	N.A.	N.A.
[35]	N.A.	8-11 GHz	0.315	1.35 dB	985 dB/Decade	5th order	Chebyshev
[36]	BSF with Two stopbands centered at 2.34 GHz and 7.81GHz with the fractional bandwidths of 33.2%, and 7.9%						
[37]	90 mm *90 mm	A compact duplex filtering antenna using a T-shape probe-fed patch and hairpin resonators (5th order). The dual-band radiation element is coupled to two bandpass filters based on half-wavelength hairpin resonators directly to construct the duplex filtering antenna.					
This work Tx	29.2 mm * 20 mm	2.2 -2.3 GHz	0.0444	2 dB	1000 dB/Decade	3rd order	Chebyshev
This work Rx	29.2 mm * 20 mm	2.04 - 2.11 GHz	0.0337	2 dB	1000 dB/Decade	3rd order	Chebyshev

TABLE 8. The corrected dimensions of the proposed Tx filter.

Parameter	Value in mm
L_m	9.76
L_f	12.92
S_1	0.2706
S_2	1.01219
W_f	2.3149
W	29.5
L	20
W_{50}	0.52

TABLE 9. The corrected dimensions of the proposed Rx filter.

Parameter	Value in mm
L_m	9.744
L_f	14
S_1	0.274
S_2	1.0138
W_f	2.3149
W	29.23
L	20
W_{50}	0.52

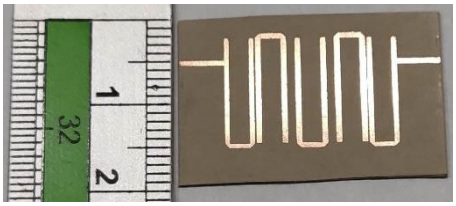

FIGURE 32. Tx filter after correction.

The small deviation between the simulated (using CST and ADS) and the measured results may be attributed to many parameters, including fabrication tolerance, connector tolerance and cable tolerance. However, they have the same resonant frequencies.

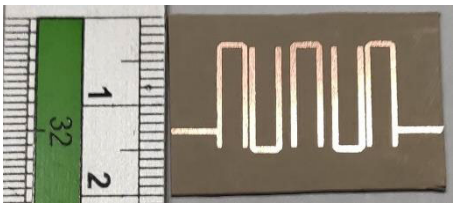

FIGURE 33. Rx filter after correction.

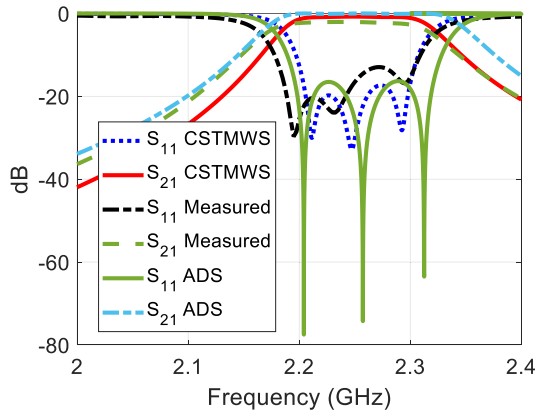

FIGURE 34. Tx filter after correction.

The proposed filters are 3rd order Chebyshev Tx, and Rx filters with a high roll-off compared to that in literature [28]–[34] which have at least similar order or higher. The filters exhibit narrow fractional bandwidth of 0.0444, and 0.0337, respectively compared to those in literature [28]–[34].

V. RF, AND FPGA BOARDS

The remaining components of the proposed CubeSat transceiver subsystem are; the FPGA board, RF transceiver, and power amplifier board.

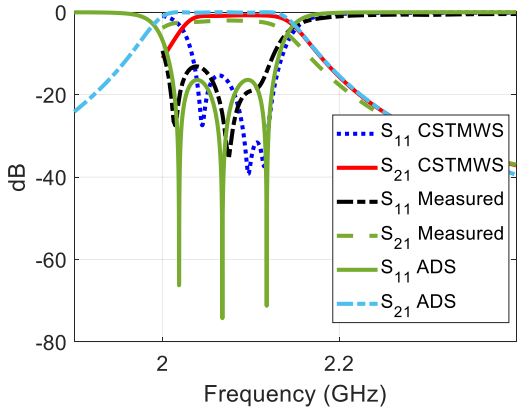

FIGURE 35. Rx filter after correction.

In order to allow parallel processing for data, a reconfigurable logic device, FPGA, is utilized. The communication board uses the AD9361 RF transceiver. The design includes zynq-7000 FPGA to control the system and the RF transceiver for generating waveforms and to receive the RF signal. Also, the design includes 512 MB DDR3 RAM for saving the data to be processed.

In order to meet the calculated link budget, the output of the RF transceiver should be amplified to get an output power of around 2 Watts.

The amplification of the RF signal Stage, consisting of the RFPA2016 3-Stage Power Amplifier, 2W 700MHz to 2700MHz (QORVO Company). The output power of the RF power amplifier is 2 Watt (33dBm). The proposed frequency range lies in the S-band frequency band (from 2.025 to 2.29 GHz). So, the amplifier achieves the required band.

VI. CONCLUSION

The research in this paper conducts the design of a CubeSat transceiver in the S-band due to its high bandwidth that suits the images, and videos transmission between the satellites, and the ground stations. The overall system layout is introduced with the main focus on both the antenna and filters design.

The two passive components achieve the required bandwidth; from 2.2 GHz to 2.29 GHz, and from 2.025 GHz to 2.11 GHz for the downlink, and the uplink, respectively. The antenna and filters achieve the required specifications for the proposed CubeSat communication subsystem. The other components are carefully selected to meet the required specifications. The antenna and filters are designed, fabricated, and measured where good results are achieved.

REFERENCES

[1] K. Woellert, P. Ehrenfreund, A. J. Ricco, and H. Hertzfeld, "Cubesats: Cost-effective science and technology platforms for emerging and developing nations," *Adv. Space Res.*, vol. 47, no. 4, pp. 663–684, Feb. 2011.

[2] F. Davoli, C. Kourogiorgas, M. Marchese, A. Panagopoulos, and F. Patrone, "Small satellites and cubeSats: Survey of structures, architectures, and protocols," *Int. J. Satell. Commun. Netw.*, vol. 37, no. 4, pp. 343–359, 2018.

[3] A. Q. Rogers and R. A. Summers, "Creating capable nanosatellites for critical space missions," *Johns Hopkins APL Tech. Dig.*, vol. 29, no. 3, pp. 283–288, 2010.

[4] S. Lee, "CubeSat design specification rev 13: The CubeSat program" California Polytech. State Univ., San Luis Obispo, CA, USA, Tech. Rep., 2014. [Online]. Available: https://www.cubesat.org

[5] A. Kyrgiazos, B. Evans, P. Thompson, P. Mathiopoulos, and S. Papaharalabos, "A terabit/second satellite system for European broadband access: A feasibility study," *Int. J. Satell. Commun. Netw.*, vol. 32, no. 2, pp. 63–92, 2014.

[6] S. Lee, A. Hutputanasin, and A. Toorian, "CubeSat design specification. Rev. 13: The CubeSat program," California Polytech. State Univ., San Luis Obispo, CA, USA, Tech. Rep., 2014.

[7] Y. Rahmat-Samii, V. Manohar, and J. M. Kovitz, "For satellites, think small, dream big: A review of recent antenna developments for CubeSats," *IEEE Antennas Propag. Mag.*, vol. 59, no. 2, pp. 22–30, Apr. 2017.

[8] F. E. Tubbal, R. Raad, and K.-W. Chin, "A survey and study of planar antennas for pico-satellites," *IEEE Access*, vol. 3, pp. 2590–2612, 2015.

[9] R. Montaño, N. Neveu, S. Palacio, E. Martinez, D. R. Jackson, J. Chen, P. W. Fink, and R. S. Provence, "Development of low-profile antennas for CubeSats," in *Proc. 28th Annu. AIAA/USU Conf. Small Satell.*, Logan, UT, USA, Aug. 2014, pp. 1–5.

[10] T. Yasin and R. Baktur, "Circularly polarized meshed patch antenna for small satellite application," *IEEE Antennas Wireless Propag. Lett.*, vol. 12, pp. 1057–1060, 2013.

[11] B. K. Montgomery, S. K. Podilchak, and Y. M. M. Antar, "Circularly polarized meshed patch antenna for cubesats and other small sattelites," in *Proc. IEEE Int. Symp. Antennas Propag. (APSURSI)*, Jun./Jul. 2016, pp. 1547–1548.

[12] X. Liu, J. Liu, D. R. Jackson, J. Chen, P. W. Fink, and G. Y. Lin, "Broadband transparent circularly-polarized microstrip antennas for CubeSats," in *Proc. IEEE Int. Symp. Antennas Propag. (APSURSI)*, Jun./Jul. 2016, pp. 1545–1546.

[13] A. Budianu, A. Meijerink, M. J. Bentum, D. M. P. Smith, and A.-J. Boonstra, "Antenna architecture of a nano-satellite for radio astronomy," in *Proc. IEEE Aerosp. Conf.*, Mar. 2014, pp. 1–10.

[14] G. F. Kurnia, B. S. Nugroho, and A. D. Prasetyo, "Planar inverted-F antenna (PIFA) array with circular polarization for nano satellite application," in *Proc. Int. Symp. Antennas Propag. Conf.*, Dec. 2014, pp. 431–432.

[15] G. Dassano and M. Orefice, "The PICPOT satellite antenna systems," in *Proc. IEEE Antennas Propag. Soc. Int. Symp.*, Jun. 2007, pp. 3029–3032.

[16] E. Pittella, S. Pisa, M. Pontani, A. Nascetti, P. D'Atanasio, A. Zambotti, and H. Hadi, "Reconfigurable S-band patch antenna system for CubeSat satellites," *IEEE Aerosp. Electron. Syst. Mag.*, vol. 31, no. 5, pp. 6–13, May 2016.

[17] A. Nascetti, E. Pittella, P. Teofilatto, and S. Pisa, "High-gain S-band patch antenna system for earth-observation CubeSat satellites," *IEEE Antennas Wireless Propag. Lett.*, vol. 14, pp. 434–437, 2015.

[18] Q. Wu, H. Wang, C. Yu, X. Zhang, and W. Hong, "L/S-band dual-circularly polarized antenna fed by 3-dB coupler," *IEEE Antennas Wireless Propag. Lett.*, vol. 14, pp. 426–429, 2015.

[19] E.-C. Choi, J. W. Lee, T.-K. Lee, and W.-K. Lee, "Circularly polarized S-band satellite antenna with parasitic elements and its arrays," *IEEE Antennas Wireless Propag. Lett.*, vol. 13, pp. 1689–1692, 2014.

[20] S. M. Hasan, M. Samsuzzaman, M. Rana, T. Islam, and T. Islam, "Circularly polarized S band patch antenna for small satellite application," in *Proc. IEEE Int. Conf. Telecommun. Photon. (ICTP)*, Dhaka, Bangladesh, Dec. 2017, pp. 200–204.

[21] A. H. Lokman, P. J. Soh, S. N. Azemi, M. F. Jamlos, A. A. Al-Hadi, S. Chalermwisutkul, and P. Akkaraekthalin, "Compact circularly polarized S-band antenna for pico-satellites," in *Proc. Int. Symp. Antennas Propag. (ISAP)*, Phuket, Thailand, Oct. 2017, pp. 1–2.

[22] S. Liu, P. I. Theoharis, F. E. Tubbal, and R. Raad, "S-band steerable Yagi antenna for CubeSats," in *Proc. 13th Int. Conf. Signal Process. Commun. Syst. (ICSPCS)*, Gold Coast, QLD, Australia, Dec. 2019, pp. 1–5.

[23] F. Tubbal, R. Raad, K.-W. Chin, L. Matekovits, B. Butters, and G. Dassano, "A high gain S-band slot antenna with MSS for CubeSat," *Ann. Telecommun.*, vol. 74, nos. 3–4, pp. 223–237, Nov. 2018.

[24] F. E. Tubbal, R. Raad, and K.-W. Chin, "A wideband F-shaped patch antenna for S-band CubeSats communications," in *Proc. 10th Int. Conf. Signal Process. Commun. Syst. (ICSPCS)*, Gold Coast, QLD, Australia, Dec. 2016, pp. 1–4.

[25] M. Hwang, G. Kim, S. Kim, and N. S. Jeong, "Origami-inspired radiation pattern and shape reconfigurable dipole array antenna at C-band for CubeSat applications," *IEEE Trans. Antennas Propag.*, early access, Oct. 20, 2020, doi: 10.1109/TAP.2020.3030908.

[26] J. M. Veljovic and K. A. Skrivervik, "Origami-inspired radiation pattern and shape reconfigurable dipole array antenna at C-band for CubeSat applications," *IEEE Trans. Antennas Propag.*, vol. 67, no. 5, pp. 3439–3444, May 2019.
[27] D. M. Pozar, *Microwave Engineering*. 4th ed. Hoboken, NJ, USA: Wiley, 2012.
[28] V. K. T. Jayanthy, "Design of microstrip hairpin band pass filter using defected ground structure and open stubs," in *Proc. Int. Conf. Inf. Electron. Eng. (IPCSIT)*, vol. 6, 2011.
[29] J. S. Hong and M. J. Lancaster, *Microstrip Filters for RF/Microwave Applications*. Hoboken, NJ, USA: Wiley, 2001, pp. 12–158.
[30] A. A. Sulaiman, M. F. Ain, S. I. S. Hassan, A. Othman, M. A. Othman, R. A. Majid, M. Z. Saidin, M. H. A. Hamid, M. H. Jusoh, Z. I. Khan, N. H. Baba, R. A. Awang, Z. Awang, N. A. Z. Zakaria, and M. K. A. Mahmood, "Design of hairpin band pass filters for K-band application," in *Proc. IEEE Int. RF Microw. Conf.*, Kuala, Lumpur, Dec. 2008, pp. 23–26.
[31] R. Ahmed, S. Emiri, and Ş. T. Ímeci, "Design and analysis of a band-pass hairpin filter," in *Proc. Int. Appl. Comput. Electromagn. Soc. Symp. (ACES)*, Denver, CO, USA , Mar. 2018, pp. 1–2.
[32] A. Zakharov, S. Rozenko, and M. Ilchenko, "Varactor-tuned microstrip bandpass filter with loop hairpin and combline resonators," *IEEE Trans. Circuits Syst. II, Exp. Briefs*, vol. 66, no. 6, pp. 953–957, Jun. 2019.
[33] L. Zhou, Z. Long, H. Li, T. Zhang, and M. Qiao, "Design of an ultrawide stopband HTS LPF based on interdigital hairpin structure," *IEEE Microw. Wireless Compon. Lett.*, vol. 28, no. 8, pp. 666–668, Aug. 2018.
[34] G. M. Aristarkhov, I. N. Kirillov, A. V. Markovsky, and V. A. Pustovalova, "Compact highly selective microstrip filters with folded hairpin resonators," in *Proc. Syst. Signals Generating Process. Field Board Commun.*, Moscow, Russia, Mar. 2020, pp. 1–4.
[35] B. Mahnoor and A. I. Najam, "Design of compact wideband microstrip filter for phased array radar applications," in *Proc. 17th Int. Bhurban Conf. Appl. Sci. Technol. (IBCAST)*, Islamabad, Pakistan, Jan. 2020, pp. 611–616.
[36] J. Dzhumamuhambetov, A. Bakitgul, and A. Gorur, "A novel dual-band microstrip bandstop filter based on stepped impedance hairpin resonators," *Prog. Electromagn. Res. Lett.*, vol. 84, pp. 139–146, Jun. 2019.
[37] J. Yuan and Z. Xie, "A compact duplex filtering antenna using a T-shape probe-fed patch and hairpin resonators," *Microw. Opt. Technol. Lett.*, vol. 61, no. 11, pp. 2506–2512, Nov. 2019.

HAYTHEM HUSSEIN ABDULLAH received the B.Sc. degree in electronics and communication engineering from the University of Benha, Egypt, in 1998, and the M.Sc. and Ph.D. degrees from Cairo University, in 2003 and 2010, respectively. His M.Sc. is dedicated to the simulation of the dispersive materials in the finite difference time domain numerical technique and its application to the SAR calculations within the human head. His Ph.D. is dedicated to radar target identification. He is currently employed as an Associate Professor and a former Head of the Nanotechnology Laboratory, Electronics Research Institute (ERI), Cairo, Egypt. He was the PI of two projects funded by different funding agencies. He has participated in 13 research projects at the national and international levels under Egypt–NSF–USA joint funds program, NTRA, STDF, National Authority of Remote Sensing, and so on. His current research interests include design and optimization of microstrip antenna arrays and their applications.

AYMAN ELBOUSHI (Senior Member, IEEE) was born in Zagazig, Egypt, in 1978. He received the B.Sc. degree in electrical engineering from Zagazig University, Egypt, in 2000, the M.Sc. degree from Ain Shams University, Cairo, Egypt, in 2007, and the Ph.D. degree from Concordia University, Montreal, Canada, in 2014. From 2014 to 2017, he was working as an Antenna Group Leader with the MARS Laboratory, PSATRI Institute, Riyadh, Saudi Arabia. He is currently working as a Researcher with the Electronics Research Institute (ERI), Cairo.

AHMED ESSAM GOHAR was born in Damietta, Egypt, in 1994. He received the B.Sc. degree in electronics and communication engineering from the Higher Institute of Engineering and Technology in New Damietta, Damietta, Egypt, in 2017. He is currently pursuing the M.Sc. degree with Mansoura University, in 2019. His M.Sc. aims to improve beam formation of synthetic aperture radar (SAR) antenna for SAR Satellite applications. He has been involved as a Research Assistant for many projects with the Electronics Research Institute (ERI) and the Egyptian Space Agency (EgSA). He is currently working on the design and implementation of the CubeSat antenna project as well as a C-band radar antenna array for SAR satellites.

ESMAT A. ABDALLAH (Member, IEEE) received the B.Sc., M.Sc., and Ph.D. degrees from the Faculty of Engineering, Cairo University, Giza, Egypt, in 1968, 1972, and 1975, respectively. She was nominated as an Assistant Professor, an Associate Professor, and a Professor, in 1975, 1980, and 1985, respectively. She was appointed as a President of the Electronics Research Institute (ERI), Cairo, Egypt, in 1989, a position she held for about ten years. From 1999 to 2006, she became the Head of the Microstrip Department, ERI. She is currently with the Microstrip Department, ERI. She has focused her research on microwave circuit designs, planar antenna systems, and nonreciprocal ferrite devices, and recently on EBG structures, UWB components and antenna and RFID systems. She acts as a single author and as a coauthor on more than 260 research articles in highly cited international journals and in proceedings of international conferences in her field. She supervised more than 70 M.Sc. and Ph.D. thesis. She was a PI of more than 26 projects funded from different funding agencies. She has participated in many research projects at the national and international levels under Egypt–NSF–USA joint funds program, the European Committee Programs FP7 program, NTRA, STDF, and so on. She is also a Reviewer for many international societies. She was the author of published books and chapters in books in her field of interest. She also participated in many patents.